



# CHORUS

This is the accepted manuscript made available via CHORUS. The article has been published as:

## Growing large nanostructured superlattices from a continuum medium by sequential activation of self-assembly

Zhouzhou Zhao and Wei Lu

Phys. Rev. E **83**, 041610 — Published 22 April 2011

DOI: [10.1103/PhysRevE.83.041610](https://doi.org/10.1103/PhysRevE.83.041610)

# **Growing large nanostructured superlattices from a continuum medium by sequential activation of self-assembly**

Zhouzhou Zhao and Wei Lu\*

Department of Mechanical Engineering, University of Michigan, Ann Arbor, Michigan 48109

\* To whom correspondence should be addressed: [weilu@umich.edu](mailto:weilu@umich.edu)

## ABSTRACT

We propose a mechanism to grow a large superlattice of phase domains from a continuum homogenous binary film by sequential activation of self-assembly. Self-assembly was initiated in a small mobile region (where atoms could diffuse) to form a seed pattern, and then the mobile region was shifted gradually. This process led to a long-rang ordered superlattice regardless whether the seed was perfect or not, since the pattern quickly improved to a perfect superlattice along with the sequential activation. At bistable state the scanning velocity controlled the type of superlattice. Further exploration led to an intriguing finding which we call the self-activation of self-assembly, a domino effect where the self-assembly in a small region causes a long-range interaction that destabilizes its homogeneous neighbor and triggers the propagation of self-assembly to the entire system.

PACS numbers: 68.43.Hn, 68.43.Jk, 81.16.Dn

## I. INTRODUCTION

The self-assembly of nanostructures enables a wide range of applications from nanoelectronic devices [1], ultrasensitive biosensors [2], carriers for drug delivery [3], to advanced materials with unique mechanical [4], electrical [5] or photonic [6] properties. Depending on the type of building blocks, self-assembled systems can be classified into two categories: discrete and continuum. A discrete system uses pre-fabricated building blocks with fixed sizes and shapes. Examples include the self-assembly of nanoparticles [5, 7, 8], nanorods [9, 10] and nanoplates [11, 12]. In contrast, a continuum system exploits the spontaneous formation of nanoscale domains. Examples include self-assembled domain patterns in binary monolayers [13], block copolymers [14] and organic molecular adsorbates on metal surfaces [15]. A continuum system offers several unique features. For instance, domains and their patterns self-assemble simultaneously, so that there is no need to pre-synthesize the building blocks; a significant degree of process flexibility and control can be achieved; and the approach may be applied to diverse systems.

The lack of long-range order has been a major challenge for self-assembled nanostructures since high regularity is crucial to many applications [16, 17]. Recently, the integration of self-assembly with the traditional “top-down” approach has been exploited to improve the long-range order. This approach uses templates to help a self-assembly process by modulating the energy profile. For instance, geometric templates have been used to guide the self-assembly of block copolymers [18], quantum dots [19, 20], and nanocrystals [21]. The templating approach typically requires lithography to fabricate a pre-patterned substrate or mask as a template. The wavelength of the template has to be small enough to provide effective guidance and the overall pattern is limited by the size of the template. In this paper we propose a

general kinetics-based template-free approach to grow nanostructured superlattices over a very large area.

The essence of our approach is sequential activation of self-assembly. The idea is illustrated in Fig. 1. A binary monolayer is used as an example, which may separate into two phases and self-assemble into domain patterns such as a hexagonal lattice of dots. Typically multiple grains of dots will form due to simultaneous self-assembly at different locations, producing a pattern lack of long-range order. Here we propose to first activate self-assembly in a finite mobile region, where atoms are allowed to diffuse and form domain patterns. This initial mobile region will serve as a “seed”. The seed does not need to have a perfect lattice. We then shift the mobile region like scanning. The self-assembly in the newly activated region will be influenced by the pattern already formed in the seed. In experiments, we envision that this process can be achieved by laser or ion beam scanning to control the local temperature, so that diffusion is activated sequentially at each spot along the scanning path. We show that this sequential activation will lead to a large long-rang ordered domain pattern even if we start with an imperfect seed. The pattern quickly improves and converges to a perfect superlattice along with the sequential activation. Note that sequential activation of self-assembly is different from crystal growth. The former expands by the simultaneous formation and ordering of domains through long-range interactions, while the latter grows by the local attachment of atoms with a fixed size and interatomic distance.

More interestingly, the self-activation of self-assembly can be achieved under certain conditions. In other words, the self-assembly in a small region may induce a domino effect and produce a perfect lattice expanding spontaneously without the need of explicit sequential activation such as laser scanning. This mechanism may motivate new ideas such as self-repairing

devices where self-assembly can be triggered by environment, or self-assembled drugs that form *in situ* in response to antimicrobial resistance. It may also promote thoughts in remotely analogous systems such as social events that propagates in certain ordered way through long-range interactions when a threshold is reached.

## II. THEORETICAL FRAMEWORK

A wide variety of continuum self-assembled systems demonstrate similar domain patterns, suggesting a possible universal framework to capture the essential mechanism. Here we use a phase field model to describe the formation of these patterns [22]. To explain this idea, we consider a two dimensional epilayer of two atomic species A and B, which occupies the  $x_1-x_2$  plane and forms a coherent lattice with the substrate. Experiments have shown that the composition often modulates in the plane of the layer, and the layer may separate into two phases, forming periodic dots or other regular domain patterns [13, 23]. The domain size may be in the range of 1-100nm, and stable against coarsening. Define  $C$  as the concentration fraction of B, where  $C=0$  represents pure A, and  $C=1$  represents pure B. The phase separation leads to A-rich and B-rich domains. The pattern is expressed by a spatial function  $C(x_1, x_2)$ , or  $C(\mathbf{x})$ . The free energy of the system is determined by the short-range atomic/molecular interaction and the long-range interaction between domains [24], which is given by

$$G = \int_A g(C)dA + h \int_A |\nabla C|^2 dA - \frac{1}{2} \int_A (\sigma_{31}u_1 + \sigma_{32}u_2) dA. \quad (1)$$

The first term represents the chemical energy of the epilayer per unit area, which drives phase separation. The second term represents the phase boundary energy, where  $h$  is a positive material

constant. This term prefers a larger domain size. The third term captures the long-range interaction, which prefers a smaller domain size. These two competing actions lead to the formation of a periodic pattern of alternating A-rich and B-rich domains, and the domain size is determined by their relative strength. Here  $\sigma_{31}$ ,  $\sigma_{32}$  are the traction forces per unit area on the substrate, and  $u_1, u_2$  are the corresponding displacements. The integration extends over the epilayer.

The form of the long-range interaction in Eq (1) is representative. The elastic interaction is dipole type, where the energy has  $1/r^3$  dependence ( $r$  is the distance between to interacting points). Such an interaction is quite common in nature. To account for a layer of polar molecules with electric dipoles, one can simply replace the third term with  $1/2 \int_A p_3 E_3 dA$ . Here  $p_3$  is the electric dipole moment per area, and  $E_3$  is the corresponding electric field associated with the dipole distribution. While different in the physical origin, the interaction term shows a similar mathematical structure. Thus the discussion below applies to a wide range of systems.

Domain patterns emerge by a diffusion process to reduce the free energy. The diffusion flux,  $\mathbf{J}$ , is proportional to the gradient of chemical potential,  $\mu = \delta G / \delta C$ , namely  $\mathbf{J} = -M(\mathbf{x}) \nabla \mu$ . To consider regionally activated self-assembly, we allow the mobility  $M(\mathbf{x})$  to be position-dependent. We take  $M(\mathbf{x}) = M_0$  in the activated region, where  $M_0$  is the mobility for diffusion, and  $M(\mathbf{x}) = 0$  in other regions. Substituting the diffusion flux into the mass conservation equation,  $\Lambda \partial C / \partial t + \nabla \cdot \mathbf{J} = 0$ , where  $\Lambda$  is the number of atomic sites per unit area, gives a diffusion equation [22],

$$\frac{\partial C}{\partial t} = \frac{1}{\Lambda^2} \nabla \cdot \left( M \nabla \left( \frac{\partial g}{\partial C} - 2h \nabla^2 C + \phi \varepsilon_{\beta\beta} \right) \right). \quad (2)$$

Here  $\phi$  is the surface stress difference of the two species, and  $\varepsilon_{\beta\beta} = -(1-\nu^2)\phi R / \pi E$  is the surface strain with  $E$  being the Young's modulus and  $\nu$  the Poisson's ratio.  $R$  is an area integration characterizing the long range interaction, which is given by

$$R = \iint \frac{(x_1 - \xi_1) \frac{\partial C}{\partial \xi_1} + (x_2 - \xi_2) \frac{\partial C}{\partial \xi_2}}{\left[ (x_1 - \xi_1)^2 + (x_2 - \xi_2)^2 \right]^{3/2}} d\xi_1 d\xi_2 \quad (3)$$

To describe phase separation, one can take any double well function for  $g(C)$ . We take a regular solution,  $g(C) = g_A(1-C) + g_B C + \Lambda k_B T [C \ln C + (1-C) \ln(1-C) + \Omega C(1-C)]$ , where  $g_A$  or  $g_B$  is the chemical energy of pure A or pure B. The first two terms in the bracket result from the entropy of mixing, and the third term from the energy of mixing. The dimensionless number  $\Omega$  measures the exchange energy relative to the thermal energy  $k_B T$ , where  $k_B$  is the Boltzmann constant and  $T$  is temperature.

Equation (2) can be written in a dimensionless form by scaling the coordinates with  $\sqrt{h / \Lambda k_B T}$  and the time with  $h / M_0 (k_B T)^2$ , which gives

$$\frac{\partial C}{\partial t} = \nabla \cdot \left( M \nabla \left[ P(C) - 2 \nabla^2 C - \frac{Q}{\pi} R \right] \right). \quad (4)$$

Here  $M$  is a normalized mobility taking values of 0 or 1,  $P(C) = \ln[C / (1-C)] + \Omega(1-2C)$ , and  $Q = b / l$  is the ratio of characteristic scale of domain width,  $b = \sqrt{h / \Lambda k_B T}$ , and size,  $l = Eh / (1-\nu^2) \phi^2$ .

The diffusion equation has a simple form in Fourier space,

$$\frac{\partial \hat{C}}{\partial t} = i\mathbf{k} \cdot \{M(\mathbf{x})(i\mathbf{k}\hat{\mu})_r\}_k, \quad (5)$$

where the hat and subscript ‘k’ denote Fourier transform, ‘r’ denotes inverse Fourier transform, and  $\mathbf{k}$  is the wave number vector. The chemical potential,  $\mu = P(C) - 2\nabla^2 C - QR/\pi$ , has a Fourier transform of  $\hat{\mu} = \hat{P} + 2(k^2 - kQ)\hat{C}$ .  $P$  is a nonlinear function of  $C$ , so  $\hat{P}$  is calculated by numerical Fourier transform. A semi-implicit method [25] in Fourier space for time integration was adopted for enhanced computational stability. We added a linear term,  $\nabla^4 C$ , to both sides of Eq. (4), so that Eq. (5) became  $\partial \hat{C} / \partial t + k^4 \hat{C} = i\mathbf{k} \cdot \{M(\mathbf{x})(i\mathbf{k}\hat{\mu})_r\}_k + k^4 \hat{C}$ . The idea was to treat the  $\nabla^4 C$  ( $k^4 \hat{C}$  in Fourier space) term implicitly on the left hand side and explicitly on the right hand side. This semi-implicit approach significantly alleviated the time step constraint. Denote the time step by  $\Delta t$  and replace  $\partial \hat{C} / \partial t$  by  $(\hat{C}^{(m+1)} - \hat{C}^{(m)}) / \Delta t$ . The algorithm for  $m+1$  time is given by  $(1 + k^4 \Delta t) \hat{C}^{(m+1)} = (1 + k^4 \Delta t) \hat{C}^{(m)} + \Delta t i\mathbf{k} \cdot \{M(\mathbf{x})(i\mathbf{k}\hat{\mu})_r\}_k^{(m)}$ . Simulations were carried out with  $\Omega=1.6$ ,  $Q=1.6$ , and a calculation cell size of  $512 \times 512$  grids with a grid spacing of 1. Periodic boundary condition was applied to extend the cell to the entire plane. Initial conditions were random, i.e. the initial concentration had an average of  $C_0$  with a random fluctuation within 0.001.

### III. SEQUENTIAL ACTIVATION OF SELF-ASSEMBLY

We first demonstrate the growth of long-range ordered superlattices from a seed by sequential activation of self-assembly. Representative results are shown in Fig. 2. Rather than

placing a perfect lattice directly, we grew the seed on site. Take Fig. 2a as an example. The initial concentration was  $C_0 = 0.37$  everywhere. We assigned mobility to be 1 in the square mobile region. We evolved the entire calculation cell to  $t = 10^5$ . The constraint of kinetics led to a square seed composed of white B-rich phase in the matrix of black A-rich phase. We found that smaller seeds had fewer defects. Here we took a square seed with a size of  $192 \times 192$ , which was larger than the size of a typical single grain. Therefore defects such as misalignment and multiple grains appeared in this seed. Next we shifted the mobile region to the right, which we called scanning. The shift distance in each step was much smaller compared to the seed size, which created a continuous scanning effect. The scanning velocity was chosen to ensure ample time for new domains to develop. In simulations we shifted the mobile region by one grid spacing, allowed it to evolve for a time duration of  $10^4$ , and then shifted it further. This process gave an effective scanning velocity of  $10^{-4}$ . Figure 2b shows the structure after we scanned over the width of the calculation cell, which formed a band of nicely ordered hexagonal superlattice. Noticeably, the lattice improved to perfection along with the scanning, demonstrating the tolerance of defects in the seeds. Figures 2c and 2d show a circular seed and its growth pattern. Unlike straight boundaries in the square seed, the circular boundary does not have any fixed relevance to the grain orientation in the seed. We still obtained a nicely-ordered superlattice consistent with the prevalent orientation in the seed. These results suggest that the scanning approach is not affected by the shape of the seed. This behavior is in contrast to the geometrical templating, which relies on the boundary shape to guide self-assembly.

The seeding effect can be better understood by looking into the third term in Eq.(4), which reflects the long-range interaction through  $R$ . The field induced by the seed is key to the interaction between the modulated phases in the seed and its homogeneous neighbor where the

concentration is still uniform. To quantify the field, we calculated the  $R$  distribution as shown in Fig. 3b, which corresponds to the domain pattern in Fig. 3a. The highs and lows of the  $R$  field and the domain pattern are consistent. Outside the seed, the  $R$  field promotes phase separation so that B-rich dots emerge at the locations of high  $R$ . This preference causes the dots to form at the right spots. The  $R$  field decays quickly away from the seed. Below we refer the mobile region just ahead of the seed as growth front, which experiences a significant  $R$  effect.

We identified two scenarios that the long-range field of a seed may direct the location of new domains (dots). 1) New domains emerge at the right lattice spots during the stage of phase separation. 2) New domains emerge at locally preferred locations and then migrate to the right spots under the influence of the seed. Our simulations suggest that if the seed has a close to perfect lattice, scenario 1 dominates the process. However, when the seed contains major defects such as significant misalignment, the pattern formation process shows complicated dynamics and scenario 2 dominates. In this situation the seed can experience significant self-adjustment, since part of the seeds is mobile before the mobile region shifts completely outside of the seed region. When the portion of seed next to the growth front lacks any prevailing grain orientation, it is difficult to form a single grain lattice in the growth front to match the poly grain boundary of the seed. As a result, new domains emerge at locally preferred locations. This disordered region, including the growth front and the portion of seed next to it, demonstrates realignment and local rotation to negotiate a common lattice orientation. After the lattice improves, scenario 1 dominates the following scanning.

We found the scanning velocity can control the domain pattern when the system is in a bistable state. This state refers to a window of average concentration, where both hexagonal lattice of dots and stripes can stabilize. **To better understand the behavior, we calculated the free**

energy for different phases, including homogeneous, hexagonal, stripe, and mixed patterns. The average energy per unit area depends on material properties and the average concentration,  $C_0$ . For a given material system, the average energy density can be expressed by  $\Lambda k_B T \cdot \tilde{g}(C_0)$ , where  $\tilde{g}$  is dimensionless. The equilibrium pattern is determined by minimizing  $\tilde{g}$ . To compute  $\tilde{g}(C_0)$ , we consider a concentration field represented by a Fourier series, namely,

$$C = C_0 + \sum_m q_{m0} \cos\left(m \frac{2\pi x_1}{\tilde{d}}\right) + \sum_n q_{0n} \cos\left(n \frac{2\pi x_2}{\sqrt{3}\tilde{d}}\right) + \sum_{m,n} q_{mn} \cos\left(m \frac{2\pi x_1}{\tilde{d}}\right) \cos\left(n \frac{2\pi x_2}{\sqrt{3}\tilde{d}}\right), \quad (6)$$

where the summation runs from 1 to  $\infty$ . This expression describes a hexagonal pattern of dots lining up along the  $x_1$  direction, as shown in the inset of Fig. 4a. Here  $\tilde{d}$  is the normalized distance between dots. The physical distance is given by multiplying the length scale, i.e.  $b\tilde{d}$ . Note that this expression can also represent stripe patterns if we only retain the first two terms in Eq. (6), where  $\tilde{d}$  becomes the distance between two stripes. We seek coefficients  $\tilde{d}$ ,  $q_{m0}$ ,  $q_{0n}$ ,  $q_{mn}$  to minimize the free energy. This process would give the equilibrium distance and shape of dots or stripes. The corresponding minimized energy is the free energy for the dot or stripe phases.

Combining Eq. (1) and (6) gives

$$\tilde{g} = L + \frac{S}{2} \left(\frac{2\pi}{\tilde{d}}\right)^2 - \frac{QH}{2} \left(\frac{2\pi}{\tilde{d}}\right), \quad (7)$$

where  $L = \int_{-1/2}^{1/2} \int_{-1/2}^{1/2} [C \ln C + (1-C) \ln(1-C) + \Omega C(1-C)] d\xi_1 d\xi_2$ ,  $\xi_1 = x_1 / \tilde{d}$ ,  $\xi_2 = x_2 / \sqrt{3}\tilde{d}$ ,  $S = \sum_m m^2 q_{m0}^2 + \sum_n n^2 q_{0n}^2 / 3 + 1/2 \sum_{m,n} (m^2 + n^2 / 3) q_{mn}^2$ , and

$H = \sum_m m q_{m0}^2 + \sum_n n q_{0n}^2 / \sqrt{3} + 1/2 \sum_{m,n} q_{mn}^2 \sqrt{m^2 + n^2} / 3$  depend only on the geometry, and not the scale, of the patterns. By minimizing  $\tilde{g}$  in terms of  $\tilde{d}$ , namely  $\partial\tilde{g}/\partial\tilde{d} = 0$ , we obtain the equilibrium size  $\tilde{d} = 4\pi S / QH$ . This equation combined with Eq. (7) gives

$$\tilde{g} = L - \frac{Q^2 H^2}{8S}. \quad (8)$$

We minimize Eq. (8) with respect to  $q_{m0}$ ,  $q_{0n}$ , and  $q_{mn}$  by the conjugate-gradient method to obtain the free energy of the dot phase. For the stripe phase we only retain the first two terms in Eq. (6) and minimize Eq. (8) with respect to  $q_{m0}$ . For the homogenous phase the free energy is simply  $L$  evaluated at the uniform concentration,  $C = C_0$ .

Figure 4a shows the phase energy of hexagonal and stripe patterns as well as the homogenous phase with a uniform concentration when  $\Omega=1.6$  and  $Q=1.6$ . When the average concentration is small, the homogenous phase is stable. Note that the curves of the hexagonal and stripe patterns all converge to the homogenous phase for small concentrations since the energy minimization of Eq. (8) automatically selects uniform concentration with vanishing  $q_{m0}$ ,  $q_{0n}$ , and  $q_{mn}$ . The common tangent of the curves for hexagonal and stripe patterns defines a window of  $0.41 < C_0 < 0.47$  where the mixed pattern is stable. The hexagonal pattern is stable for  $C_0 < 0.41$ , and the stripe pattern is stable for  $C_0 > 0.47$ . Stability analysis and simulations also revealed this window [26]. We took  $C_0$  to be 0.42 which is within the window of the bistable state. Figure 4b shows the pattern in the seed grown in the same way as that in Fig. 2. The seed consists of ordered dots with few very short stripes. However, when we scanned with the same velocity of  $10^{-4}$  as before, a band of parallel stripes formed, as shown in Fig. 4c. The slow scanning velocity allowed the pattern to evolve close to equilibrium in each scanning step. Note

that these stripes did not take over the dots in the seed, suggesting that they can coexist. In Fig. 4d, we increased the scanning velocity to 0.5. Surprisingly, a band of hexagonal lattice of dots formed. This phenomenon reflects a non-equilibrium growth mode, where new domains do not have much time to relax before the mobile region shifts. This observation suggests a new growth mechanism controlled by scanning velocity, which manipulates the competition between domain coarsening and growth. At low velocity, new domains have sufficient time to coarsen into parallel stripes, which have lower energy. Here the regular spacing of dots in the seed has provided an important guidance, since a pattern of parallel stripes is difficult to form spontaneously. At high velocity, new domains do not have much time to coarsen so that they form a lattice of dots. Figure 4f shows a ‘phase diagram’ of patterns in terms of the scanning velocity and average concentration. This diagram was obtained by calculating a series of combination of the scanning velocity and average concentration. The unique effect of kinetic guidance divides the patterns into two regimes, stripes and dots, with a transition region of mixed patterns in between.

High output is essential to nanostructure applications. We propose two schemes to facilitate large-scale fabrication. 1) As shown in Fig. 5a, we alternated the scanning directions between left-right scanning and up-down scanning, using the superlattice created in each previous step as a large seed. This scheme allowed the growth rate (area of lattice created per unit time) to increase exponentially with time, greatly accelerating large area fabrication. 2) As shown in Fig. 5b, we increased the size of the mobile area in two dimensions, rather than scanning along one direction. This scheme allowed the growth rate to be quadratic of the scanning velocity.

#### IV. SELF-ACTIVATED SELF-ASSEMBLY

An intriguing finding is that under certain condition a single grain superlattice can grow spontaneously from a seed without explicit scanning. In this case the whole surface is mobile. We suppress simultaneous self-assembly at multiple locations by choosing a low average concentration so that phase separation does not occur. In the simulations we took  $C_0$  to be 0.33, which was stable upon any small perturbation and no pattern would form. We then added material to a small region as shown in Fig. 6a, so that the concentration in the central circular area became 0.37. The diameter of the area was 10, which was about the size of one domain. Figure 6b shows that the small area became unstable and phase separation started to emerge. The process further destabilized the homogeneous neighbor of this seed, causing a domino effect which expanded the activated self-assembly region. Finally a large hexagonal superlattice formed. We found that the long-range elastic field generated by the seed is key to this self-activation of self-assembly, which provides an additional destabilizing force that causes the would-be homogenous region outside the seed to phase separate and form patterns. The process was accompanied by a diffusion of B atoms from distance to the boundary of the seed, as illustrated by the arrow in Fig. 6d.

This self-activation of self-assembly demonstrates an interesting growth behavior. New domains tend to form at the kink site as noted in Fig. 6d, where a domain has half of the nearest neighbors in a lattice. This behavior can be generally expressed by  $n = Z/2$ , where  $n$  is the actual number of nearest domains and  $Z$  is the number of nearest neighbor sites in the domain lattice. The kink sites in Fig. 6 have  $Z = 6$  and  $n = 3$ . The formation of new domains at step sites, where  $n = 2$ , is less common since forming a kink domain leads to more free energy reduction. Due to the low average concentration, forming B-rich domains will exhaust B atoms

locally segregated out of the A-rich matrix, and thus incurs diffusion of B from distance. Under this competition for B, forming kink domains slows down the possible nearby step domains. The growth rate of the repeatable kink sites does not change much along an edge of the seed, suggesting that the overall growth rate of the superlattice may be determined by a kink kinetics — dominated self-assembly process.

The effects of the kink growth and long range diffusion are reflected in Fig. 6g, which shows the size of the superlattice as a function of the growth time. The area of a superlattice scales with the number of dots in it. The growth rate characterized by area per unit time is almost constant when the growth time is less than 10000. In this time frame there is sufficient local supply of B atoms so that the growth rate is limited by the kink kinetics. This effect causes the formation of a fixed number of new dots per unit time, and therefore leads to a constant growth rate of the superlattice. The growth rate decreases as the superlattice grows larger since sustaining the growth requires the diffusion of B atoms from distance. The growth eventually stops when all the B atoms are consumed in the calculation cell to form the superlattice.

## V. CONNECTION TO REPRESENTATIVE SYSTEMS

Equations (4) and (5) are dimensionless, so that the simulation results are representative of a wide range of materials systems having different pattern size scales. A particularly interesting system is substrate-mediated spinodal decomposition of a binary epitaxial monolayer, such as lead on copper [13], oxygen on copper [23], or thin film separating into A-rich and B-rich domains. This system can also be a submonolayer of adsorbates on a substrate, where one phase is the adsorbate and the other phase is simply the bare substrate surface. Using magnitudes

$h \sim 10^{-19} \text{J}$ ,  $\Lambda \sim 5 \times 10^{19} \text{ m}^{-2}$  and  $k_B T \sim 5 \times 10^{-21} \text{ J}$  (corresponding to  $T=400\text{K}$ ), we have  $b \sim 0.6 \text{ nm}$ . In simulations a grid spacing of 1 corresponds to a physical spacing of  $b$ , which can be used to correlate the calculation cell size mentioned in previous sections to the physical size. Assuming that the Young's modulus of the substrate is  $E \sim 10^{11} \text{ N/m}^2$ , the Poisson's ratio is  $\nu \sim 0.3$ , the surface stress difference of two domains is on the order of  $\phi \sim 1-4 \text{ N/m}$  [27], we have a characteristic size scale  $l \sim 0.6-10 \text{ nm}$ . The domain size is roughly  $4\pi l$ . A larger surface stress difference, and a smaller interfacial tension and substrate stiffness lead to smaller domain sizes.

The value of  $h$  can be related to the interfacial tension,  $\gamma$ , between A-rich and B-rich domains by an integration across the interface, namely  $\gamma = h \int_{-\infty}^{\infty} (\partial C / \partial x)^2 dx$ . Experimentally the gradient in the interfacial region can be approximated by  $\Delta C / \delta$ , where  $\Delta C$  is the concentration difference of the two phases, and  $\delta$  is the interfacial thickness. This approximation gives  $h = \gamma \delta / (\Delta C)^2$ .

For a system with quite different magnitudes of  $b$  and  $l$ , it is computational intensive to resolve both the interface and multiple domains. In most cases we are interested in the domain size and patterning, when it is not necessary to resolve accurately the interfacial transition. In such situations one may treat  $b$  as a spatial resolution to be resolved in the simulation, whose value is given by  $l/Q$ . Here  $l$  is calculated from material parameters and determines the physical size scale. The parameter  $Q$  controls the spatial resolution and the number of domains to appear in a calculation cell.

Equation (4) may also be connected to other systems where the long-range interaction is electric dipole [28, 29] instead of elasticity. Examples include Langmuir films and adsorbates of

dipole molecules. The former has a typical domain size of 1–10 $\mu\text{m}$  [30] while the latter has a typical size of 1-100nm. These sizes can be converted to the characteristic size scale by the relation of  $4\pi l$ . Domain patterns are also encountered in polymeric assemblies during microphase separation [31, 32]. The connectivity of molecular blocks precludes composition modulation over large length scale, leading to an effective long range interaction similar to dipole interactions. In analogy to  $l \sim Eh/\phi^2$  for epitaxial layers, from dimensional analysis we have a characteristic scale  $l \sim \epsilon h/\eta^2$  for systems involving dipole interaction, where  $\epsilon$  is the permittivity of the media and  $\eta$  is the dipole density (electric dipole moments per unit area) difference of A-rich and B-rich domains. Thus a larger dipole density difference and a smaller interfacial tension reduce the domain sizes.

From an experimental point of view, we envision that there are several ways to achieve a sequential series of self-assembly in addition to laser scanning or thermal activation. For instance, one may translate a substrate or nozzle during local deposition, or use other fields such as light or electric field to activate self-assembly at different locations sequentially.

## VI. CONCLUSIONS

In summary, we proposed an approach of sequentially activated self-assembly to grow large-area superlattices from a continuum medium. We revealed the underlying mechanism and demonstrated the flexibility and defect tolerance of this approach. We also discovered a self-activated self-assembly mechanism where the growth of superlattice can be achieved without explicit scanning. The  $1/r^3$  long range interaction considered in this paper is representative of a range of systems such as Langmuir films, ferromagnetic films, and self-assembled monolayers.

The demonstration of self-propagation of ordering may motivate study of similar phenomena in a range of fields from physics to materials and bio-systems.

### **ACKNOWLEDGEMENTS**

The authors acknowledge financial support from National Science Foundation Award No. CMMI-0700048.

## REFERENCES

- [1] B. A. Parviz, D. Ryan, and G. M. Whitesides, *IEEE Trans. Adv. Packag.* **26**, 233 (2003).
- [2] J. M. Nam, C. S. Thaxton, and C. A. Mirkin, *Science* **301**, 1884 (2003).
- [3] Y. N. Xia, *Nat. Mater.* **7**, 758 (2008).
- [4] R. Klajn, K. J. M. Bishop, M. Fialkowski, M. Paszewski, C. J. Campbell, T. P. Gray, and B. A. Grzybowski, *Science* **316**, 261 (2007).
- [5] E. V. Shevchenko, D. V. Talapin, N. A. Kotov, S. O'Brien, and C. B. Murray, *Nature* **439**, 55 (2006).
- [6] C. Paquet, and E. Kumacheva, *Materials Today* **11**, 48 (2008).
- [7] D. Nykypanchuk, M. M. Maye, D. van der Lelie, and O. Gang, *Nature* **451**, 549 (2008).
- [8] T. P. Bigioni, X. M. Lin, T. T. Nguyen, E. I. Corwin, T. A. Witten, and H. M. Jaeger, *Nat. Mater.* **5**, 265 (2006).
- [9] H. Chik, J. Liang, S. G. Cloutier, N. Kouklin, and J. M. Xu, *Appl. Phys. Lett.* **84**, 3376 (2004).
- [10] S. Pierrat, I. Zins, A. Breivogel, and C. Sonnichsen, *Nano Lett.* **7**, 259 (2007).
- [11] S. H. Chen, Z. Y. Fan, and D. L. Carroll, *J. Phys. Chem. B* **106**, 10777 (2002).
- [12] H. T. Zhang, G. Wu, and X. H. Chen, *Langmuir* **21**, 4281 (2005).
- [13] R. Plass, J. A. Last, N. C. Bartelt, and G. L. Kellogg, *Nature* **412**, 875 (2001).
- [14] M. J. Fasolka, and A. M. Mayes, *Annu. Rev. Mater. Res.* **31**, 323 (2001).
- [15] J. C. Love, L. A. Estroff, J. K. Kriebel, R. G. Nuzzo, and G. M. Whitesides, *Chem. Rev.* **105**, 1103 (2005).
- [16] G. Hodes, *Adv. Mater.* **19**, 639 (2007).
- [17] W. A. Murray, and W. L. Barnes, *Adv. Mater.* **19**, 3771 (2007).
- [18] J. Xu, S. Park, S. L. Wang, T. P. Russell, B. M. Ocko, and A. Checco, *Adv. Mater.* **22**, 2268 (2010).
- [19] X. Mei, D. Kim, H. E. Ruda, and Q. X. Guo, *Appl. Phys. Lett.* **81**, 361 (2002).
- [20] N. W. Strom, Z. M. Wang, J. H. Lee, Z. Y. AbuWaar, Y. I. Mazur, and G. J. Salamo, *Nano. Res. Lett.* **2**, 112 (2007).
- [21] A. Ghadimi, L. Cademartiri, U. Kamp, and G. A. Ozin, *Nano Lett.* **7**, 3864 (2007).
- [22] W. Lu, and Z. Suo, *J. Mech. Phys. Solids* **49**, 1937 (2001).
- [23] K. Kern, H. Niehus, A. Schatz, P. Zeppenfeld, J. George, and G. Comsa, *Phys. Rev. Lett.* **67**, 855 (1991).
- [24] Z. Suo, and W. Lu, *J. Mech. Phys. Solids* **48**, 211 (2000).
- [25] J. Z. Zhu, L. Q. Chen, J. Shen, and V. Tikare, *Phys. Rev. E* **60**, 3564 (1999).
- [26] S. Hu, G. Nathan, F. Hussain, D. J. Kouri, P. Sharma, and G. H. Gunaratne, *J. Mech. Phys. Solids* **55**, 1357 (2007).
- [27] H. Ibach, *Surf. Sci. Rep.* **29**, 193 (1997).
- [28] W. Lu, and D. Salac, *Phys. Rev. Lett.* **94**, 146103 (2005).
- [29] Z. Suo, and W. Hong, *Proc. Natl. Acad. Sci. U. S. A.* **101**, 7874 (2004).
- [30] H. Möhwald, *Annu. Rev. Phys. Chem.* **41**, 441 (1990).
- [31] J. Chai, and J. M. Buriak, *ACS Nano* **2**, 489 (2008).
- [32] C. J. Hawker, and T. P. Russell, *MRS Bull.* **30**, 952 (2005).

## FIGURE CAPTIONS

FIG. 1. A schematic of sequential activation of self-assembly. Self-assembly is first activated in a finite mobile region, where atoms are allowed to diffuse and form domain patterns. This initial mobile region serves as a “seed”. The mobile region is then shifted like scanning. Self-assembly in the newly activated region will be under influence of patterns already formed in the seed.

FIG. 2. Growth of superlattice from seeds.  $C_0 = 0.37$ . (a) A square seed. (b) A band of nicely ordered hexagonal superlattice formed after scanning over the width. The lattice improved to perfect along with the scanning, demonstrating tolerance of defects in the seeds. (c) A circular seed. (d) Superlattice formed after scanning. The circular boundary does not have any fixed relevance to the grain orientation in the seed, suggesting that the scanning approach is not affected by the shape of the seed.

FIG. 3. How a seed affects self-assembly by the  $R$  field. (a) A seed region and its homogenous neighbor. (b) The corresponding  $R$  distribution in grey scale, brighter for higher  $R$ . This field promotes phase separation so that B-rich dots emerge at locations of high  $R$ . This preference causes the dots to form at the right lattice spots.

FIG. 4. Scanning velocity can control the domain pattern when the system is in a bistable state,  $C_0 = 0.42$ . (a) Free energy of different patterns as a function of the average concentration. (b) A square seed. (c) A band of parallel stripes formed at scanning velocity of  $10^{-4}$ . (d) A band of hexagonal lattice of dots formed at scanning velocity of 0.5. (e) A pattern diagram in terms of scanning velocity and average concentration.

FIG. 5. Two schemes for scaling-up growth. (a) Alternate the scanning directions, using the superlattice created in previous step as a large seed. (b) Increase the size of the mobile in two dimension.

FIG. 6. Self-activated self-assembly from a small region in the center. The entire plane is mobile, however, the low average concentration outside the seed prohibits any spontaneous phase separation or pattern formation. The long-range field generated by the seed destabilizes its homogeneous neighbor, causing a domino effect which extends the active self-assembly region.

(a)  $t=0$  (b)  $t=100$  (c)  $t=500$  (d)  $t=5000$  (e)  $t=1 \times 10^4$  (f)  $t=5 \times 10^4$ . (g) The size of the superlattice as a function of the growth time.

# FIGURES

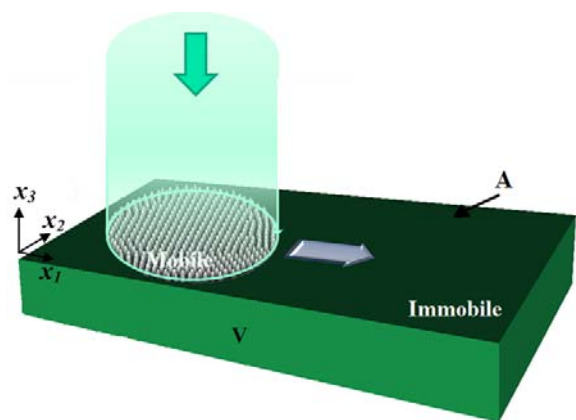


Fig. 1

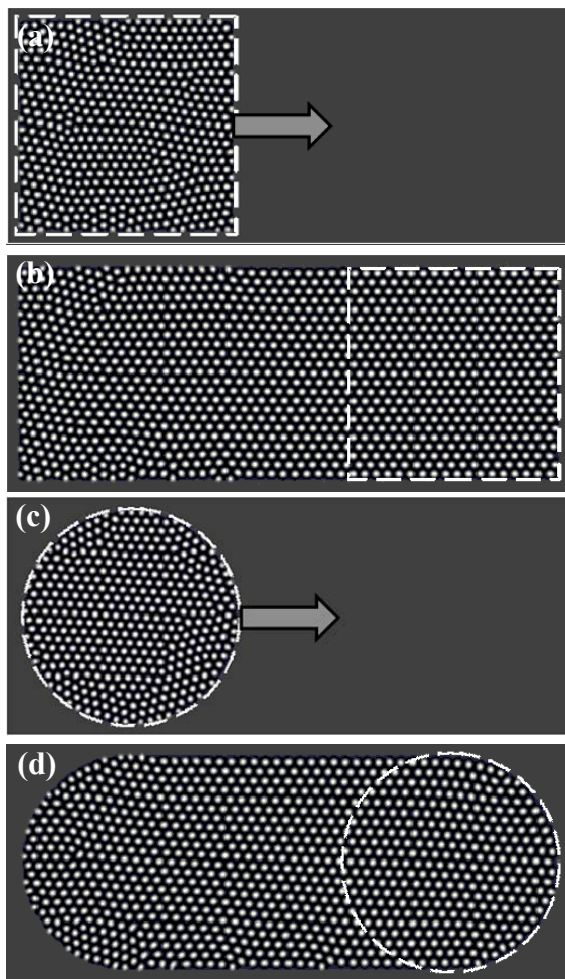


Fig. 2

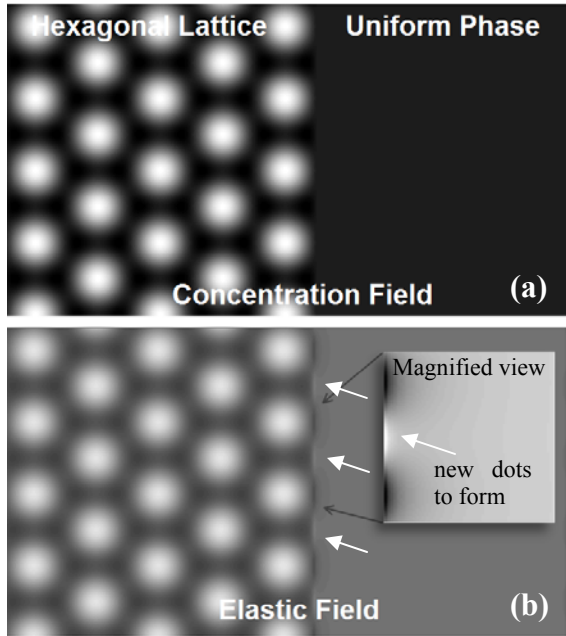


Fig. 3

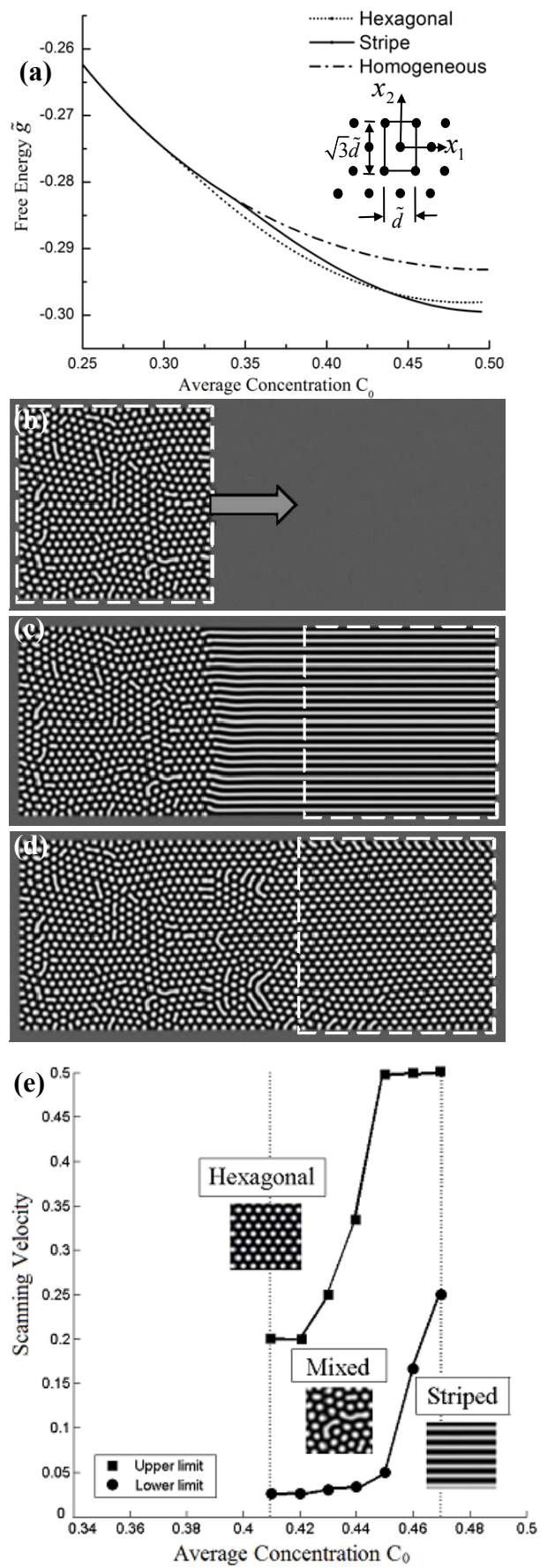


Fig. 4

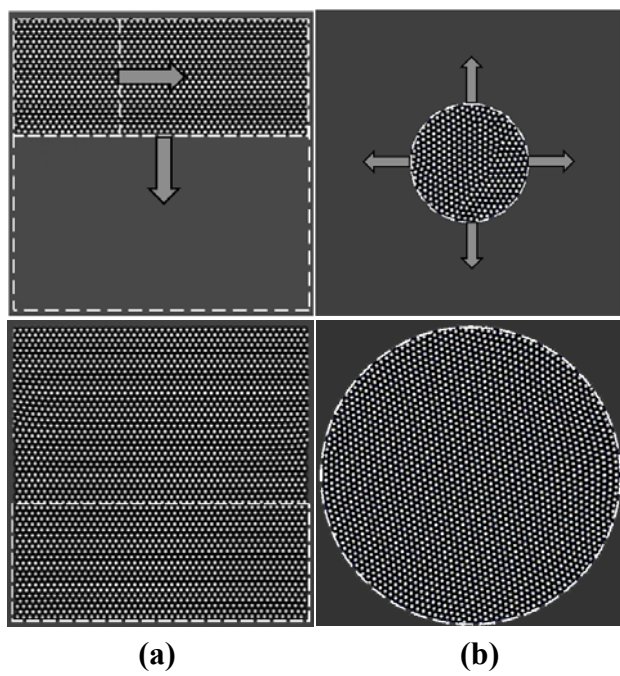


Fig. 5

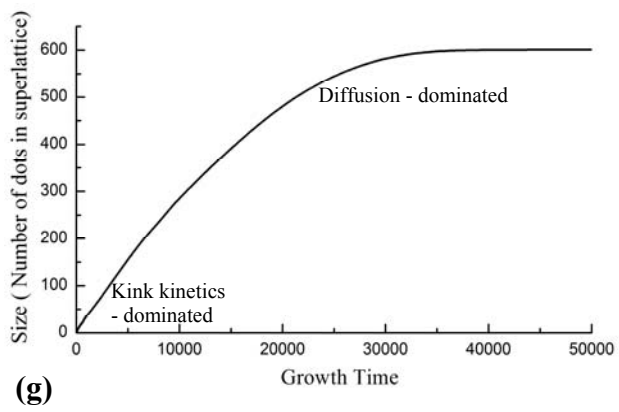
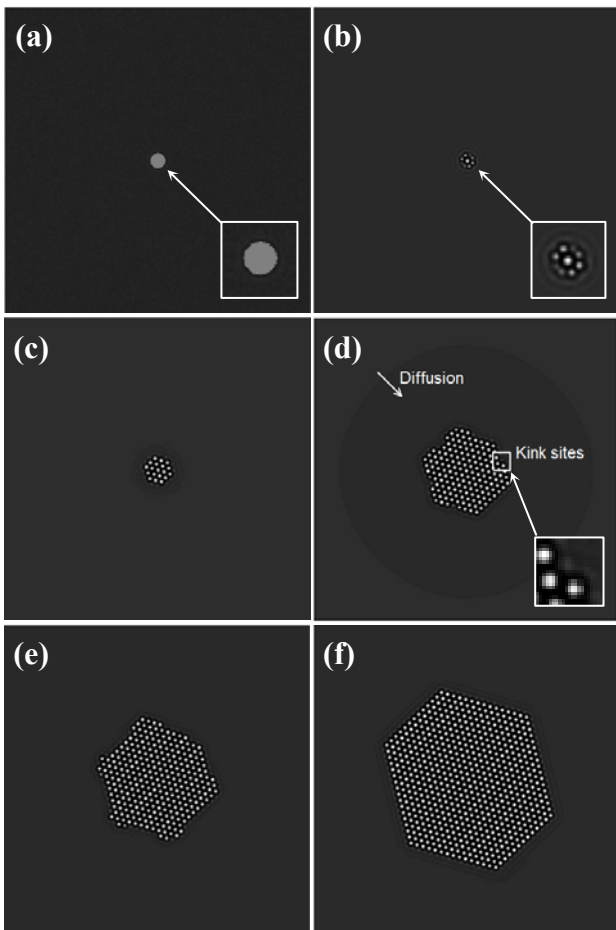


Fig. 6